Biophysical Journal
Article

Biophysical Society

Structure of Reelin repeat 8 and the adjacent C-terminal region

Liam S. Turk,[1,2,3,*] Michael J. Currie,[4] Renwick C. J. Dobson,[4,5] and Davide Comoletti[1,2,3,*]
[1]Child Health Institute of New Jersey, New Brunswick, New Jersey; [2]Department of Neuroscience and Cell Biology, Robert Wood Johnson Medical School, Rutgers, The State University of New Jersey, New Brunswick, New Jersey; [3]School of Biological Sciences, Victoria University of Wellington, Wellington, New Zealand; [4]Biomeolecular Interactions Centre and School of Biological Sciences, University of Canterbury, Christchurch, New Zealand; and [5]Bio21 Molecular and Biotechnology Institute, Department of Biochemistry and Molecular Biology, University of Melbourne, Parkville, Victoria, Australia

ABSTRACT Neuronal development and function are dependent in part on the several roles of the secreted glycoprotein Reelin. Endogenous proteases process this 400 kDa, modular protein, yielding N-terminal, central, and C-terminal fragments that each have distinct roles in Reelin's function and regulation. The C-terminal fragment comprises Reelin repeat (RR) domains seven and eight, as well as a basic stretch of 32 amino acid residues termed the C-terminal region (CTR), influences Reelin signaling intensity, and has been reported to bind to Neuropilin-1, which serves as a co-receptor in the canonical Reelin signaling pathway. Here, we present a crystal structure of RR8 at 3.0 Å resolution. Analytical ultracentrifugation and small-angle x-ray scattering confirmed that RR8 is monomeric and enabled us to identify the CTR as a flexible, yet compact subdomain. We conducted structurally informed protein engineering to design a chimeric RR8 construct guided by the structural similarities with RR6. Experimental results support a mode of Reelin-receptor interaction reliant on the multiple interfaces coordinating the binding event. Structurally, RR8 resembles other individual RRs, but its structure does show discrete differences that may account for Reelin receptor specificity toward RR6.

SIGNIFICANCE Reelin is a modular, secreted glycoprotein that drives aspects of neuronal development and function. Considerable effort has been made to understand the peripheral Reelin domains, including that of Reelin repeat 8 (RR8) and its adjacent C-terminal region (CTR), which has recently been reported to bind to Neuropilin-1. However, no structural analysis has been published regarding these sections of Reelin. Here, we 1) report the crystal structure of RR8, 2) confirm the in-solution assembly of an RR8-CTR construct using AUC, 3) identify the CTR as a structurally distinct domain using SAXS, and 4) design and purify two chimeric RR8 constructs based on the structural data presented herein that provide mechanistic information on Reelin signaling pathway activation.

INTRODUCTION

Reelin is a modular glycoprotein that is involved in several aspects of brain development and function (1–13). This large, secreted, dimeric protein interacts with the very low-density lipoprotein receptor (VLDLR) and the apolipoprotein E receptor 2 (ApoER2) to evoke most of its biological functions (14,15). Reelin comprises several domains, including eight RRs of ∼400 amino acid residues each. Reelin is subject to proteolytic cleavage, yielding three main fragments: the N-terminal fragment (NT), central fragment (CF), and C-terminal fragment (CT) (Fig. 1 *A*) (16–20). Owing to its large size and cleavage pattern, full-length (FL) Reelin has historically been difficult to work with, and therefore research groups have often focused on individual proteolytic fragments. A large amount of work has previously focused on the CF, as it contains both the lipoprotein receptor binding site and the Reelin dimerization site, enabling it to induce canonical Reelin signaling in dissociated neurons (21–24). However, there is a growing repository of research being published on the peripheral Reelin fragments and domains, showing that they, and the proteolytic events surrounding them, play biologically relevant roles (17,25–28).

The structures for RRs 1, 3, 5, and 6 have thus far been solved using x-ray diffraction (RR1 as part of a larger

Submitted May 6, 2022, and accepted for publication May 31, 2022.

*Correspondence: liam.turk@otago.ac.nz or davide.comoletti@vuw.ac.nz
Liam S. Turk's present address is Department of Biochemistry, University of Otago, Dunedin, New Zealand.

Editor: Frank Gabel.
https://doi.org/10.1016/j.bpj.2022.06.002

construct incorporating part of the NT, RR3 as an individual subunit, and RR5 and RR6 as a two-domain deletion construct) (22,25,29–31). Amino acid sequence identities between the different RRs range from ~25 to ~40%; it is therefore unsurprising that the tertiary structures between the different RRs agreeably align, with the largest root mean-square deviation (RMSD) being 2.8 Å (Fig. 1, *B* and *C*). Structurally, each RR is composed of 2 subdomains, termed A and B, that are connected by an EGF-like domain. Each subdomain is made of 11 β-strands that coalesce as 2 β-sheets in a jelly-roll-like fold. Characteristic of Reelin repeats is a structural motif known as the aspartate (D)-box or bacterial neuraminidase repeat of unknown function, which is present in each subdomain and forms a β-hairpin seen in only a handful of proteins (32).

Reelin NT is composed of an F-spondin-like domain, an "irregular" region, and RRs 1 and 2 (25,33). It has been shown to oligomerize and drive the formation of higher-order Reelin multimers that efficiently activate the canonical signaling pathway, and the proteolytic processing event that cleaves Reelin NT leads to a downregulation of Reelin activity (17,34,35). Recently, the crystal structure corresponding to the irregular region and RR1 of the NT was solved, and the group responsible also noted the F-spondin-like domain's importance in NT oligomerization (25).

As Reelin CF contains both the receptor binding site (K2467) and the dimerization site (C2101), it retains the propensity to activate the canonical signaling pathway (21,24,29). This four-domain fragment has been the target of structural biologists as well, and various techniques have been used to study the CF or its deletion constructs (22,23,31).

Reelin CT comprises RRs 7 and 8, plus a basic stretch of 32 residues, known as the C-terminal region (CTR) (36). The CTR is functionally important for Reelin signaling and secretion (37). Near the C-terminus of the CTR, four consecutive arginine residues function as a Furin recognition site, leading to the cleavage of the final six amino acids from the FL protein (28). The inclusion of these final six residues has recently been shown to mediate an interaction with Neuropilin-1 (NRP-1), which has been reported to function as a co-receptor with VLDLR, and NRP-1 has previously been shown to interact with proteins bearing arginine-rich C-termini (26,38). Despite the functional importance of RR8, its structure has yet to be solved.

Here, we report and analyze the crystal structure of RR8 solved at 3.0 Å resolution. We use complementary structural and biophysical techniques to provide a high-resolution model of RR8 and its in-solution assembly. We show that RR8 folds similarly to other Reelin repeats solved to date, and we also provide data to suggest that the Reelin CTR is a flexible yet conspicuous domain, confidently identifying it in the small-angle x-ray scattering (SAXS) data. We further analyze an amino acid loop on RR8 that is homologous to Reelin's receptor binding loop, outlining key differences in its primary and tertiary structure when compared with the receptor binding site on RR6, which contains a highly conserved patch of nonpolar amino acids that serves as a hydrophobic base, positioning K2467 in a receptor-accessible orientation. We then tested if we could engineer in the ability for RR8 to bind to Reelin receptors, ApoER2 and VLDLR, through a structurally guided loop swap with RR6. While the chimeric constructs express, are soluble in solution, and display similar biophysical profiles as RR8, they bind to neither ApoER2 nor VLDLR, suggesting that Reelin's capacity to bind to the extracellular domains of ApoER2 is dependent on more than a single interface.

MATERIALS AND METHODS

HEK293 cell culture and transfection

HEK293S GnTI$^-$ cells (from ATCC) were cultured in Dulbecco's modified Eagle's medium (DMEM), supplemented with 5% fetal bovine serum (FBS) at 37°C, 5% CO_2. Stable cell lines were generated by transfecting the cells using polyethylenimine (PEI) with the cDNA of Reelin repeat 8 and an empty pcDNA3.1 plasmid that contains the geneticin-resistant gene to add G418 resistance. Stable cell lines were selected and maintained in DMEM supplemented with 5% FBS and 800 μg/mL of G418 at 37°C, 5% CO_2. HEK293S GnTI$^-$ cells were transiently transfected with the cDNA of the RR8 construct described previously as well as the double mutant RR8 R3454A R3455A using PEI. The supernatant was collected 72 h posttransfection; SDS-PAGE, followed by western blotting, was used to determine protein expression. For transient transfections of cells in suspension, Expi293F cells were maintained in Expi293 Expression Medium at 37°C, 8% CO_2 with shaking (120 rpm), and transfected using ExpiFectamine 293 reagent (Gibco, Waltham, MA, USA).

Construct design

The amino acid sequences, corresponding to the eighth mouse Reelin repeat (residues 3052–3461), the extracellular domain of mouse VLDLR (residues 24–796), and the first splice variant of the extracellular domain of mouse ApoER2 (29–159, 286–858) were cloned into a modified pCMV6-XL4 expression vector, including a prolactin leader peptide (MDSKGSSQ KGSRLLLLLVVSNLLLCQGVVSTPVV), N-terminal FLAG tag, and C-terminal human Fc fragment. An HRV-3C protease site is located between the proteins' C-termini and the start of the Fc domain. Six residues before RR8's C-terminus there is an endogenous Furin cleavage site (RRRR) that results in the removal of the last six residues of the protein, plus the Fc domain. The R3454A and R3455A mutations to yield the RR8 RRAA construct were made using site-directed mutagenesis (Agilent, Santa Clara, CA, USA) and sequence confirmed. RR8 QQ and RR8 HT constructs were synthesized (Gene Universal, Newark, DE, USA) using the same expression vector and tagging strategy mentioned above.

Protein expression and purification

Stable cell lines expressing RR8 were expanded into Nunc TripleFlask cell culture flasks in DMEM with 2–5% FBS, and the conditioned medium containing the secreted protein was collected and replenished at regular intervals. Once enough conditioned medium was collected (~3 L), the protein was purified using anti-FLAG M2 affinity gel (Sigma, St. Louis, MO, USA). The protein-bound resin was washed (50 mM Tris [pH 8.0], 450 mM NaCl), equilibrated (50 mM Tris [pH 8.0], 150 mM NaCl), and eluted using FLAG peptide. The eluted protein was then concentrated using Vivaspin concentrators (Sartorius-Stedim, Goettingen, Germany), and size-exclusion chromatography (SEC) was used to further purify the protein in a

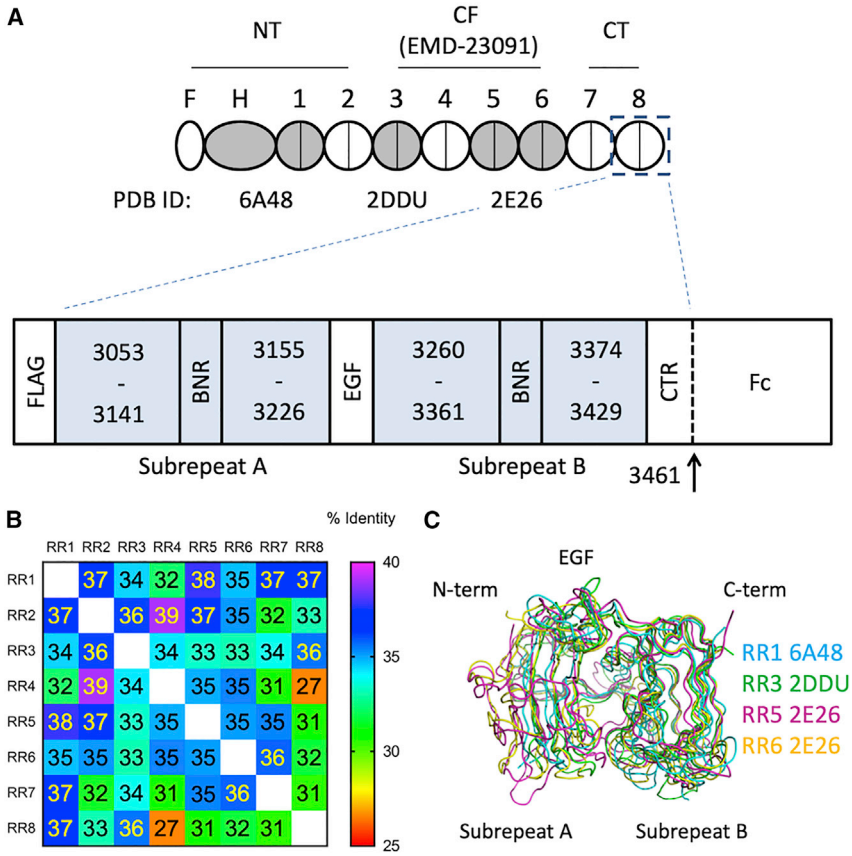

FIGURE 1 Reelin repeats share high sequence identity. (*A*) Top: schematic of full-length Reelin with three major cleavage products outlined. NT, N-terminal fragment; CF, central fragment; CT, C-terminal fragment. PDB and EMDB IDs are shown for regions for which structural information is available; domains are shaded gray if a high-resolution model is available. Bottom: schematic of RR8 construct used in this study. Subrepeat A is preceded by an N-terminal FLAG tag. Subrepeats A and B (*light blue*) both share a bacterial neuraminidase repeat (BNR) or Asp-box that forms a β-hairpin. An EGF-like domain separates subrepeats A and B. The C-terminal region (CTR) follows subrepeat B; it includes a Furin recognition site (*dashed line*) and ends at residue 3461. Human Fc is cloned in frame with the protein but is endogenously cleaved by Furin during expression of the WT protein. (*B*) Heatmap showing the degree of amino acid sequence identity between RRs. The repeats share ∼25–40% amino acid sequence identities. (*C*) Previously solved crystal structures of RR1, RR3, RR5, and RR6 show high similarity in tertiary structure when superimposed; RMSD values range from 1.3 to 2.8 Å.

Superdex 200 10/300 GL column (Cytiva, Marlborough, MA, USA), equilibrated in 50 mM Tris (pH 8.0), 150 mM NaCl, 1 mM $CaCl_2$. The protein was then concentrated to ∼10 mg/mL and either used immediately or snap-frozen in liquid nitrogen and stored at −80°C. For the expression and purification of VLDLR-Fc, ApoER2-Fc, RR8 QQ, and RR8 HT, Expi293F cells were transfected; 5 days after Expi293F transfection, the conditioned media was collected, filtered, and then purified using the same method as described above.

Crystallization and diffraction data collection

Hundreds of crystallization conditions were tested using commercial crystal screens (Hampton Research, Aliso Viejo, CA, USA) in 400 nL sitting drops using a Mosquito liquid handler (SPT Labtech, Melbourn, UK). Initial crystals were observed in 0.1 M Tris (pH 8.0), 30% PEG MME 2000, and subsequently optimized in 0.1 M Tris (pH 8.0), 35% PEG 1000. Crystals were then grown to an adequate size using the hanging-drop method, cryo-protected using 20% glycerol, and frozen in liquid nitrogen. Diffraction data of individual crystals were remotely collected on the Australian Synchrotron MX1 beamline under a 100 K cryogenic stream (39). Data were processed with XDS (40) and scaled using Aimless (41). The data were truncated to a half-set correlation ($CC_{½}$) of 0.496, corresponding to a resolution of 3.0 Å.

Structure solution and refinement

The RR8 structural solution was found through molecular replacement using the automated pipeline, MrBUMP (42) and RR6 as a search model (PDB: 2E26, residues 2326–2660, 34.2% identity). RR8 was manually modeled in Coot (43) and further refined using Phenix (44).

Analytical ultracentrifugation

Sedimentation velocity experiments were performed using a Beckman Optima XL-I analytical ultracentrifuge at the University of Canterbury's Biomolecular Interaction Center (Christchurch, New Zealand). RR8 was diluted to 0.063, 0.19, and 0.56 mg/mL (corresponding to 0.1, 0.3, and 0.9 OD, respectively) in 50 mM Tris (pH 8.0), 150 mM NaCl, 1 mM $CaCl_2$. Data were collected at 20°C. Reference (buffer) and samples were added to 12-mm double sector cells with sapphire windows, and they were run in an An-60 Ti rotor at 50,000 rpm and scanned at 287 nm. Data were analyzed using UltraScan-III v. 4.0, release 6113. UltraScan estimated the partial specific volume of RR8 to be 0.718 mL/g from the protein's sequence, analogous to Laue et al.'s outlined methods (45). The effect of glycosylation on the partial specific volume was not analyzed as the data clearly pointed to a monomeric protein. Data were analyzed using an iterative two-dimensional analysis (46,47).

CTR modeling

The tertiary structure of Reelin's final 30 amino acids up to the endogenous Furin site (V^{3426}-R^{3455}) was modeled using the predictive, template-based protein structure modeling server, RaptorX (48). The model was then manually appended to the crystal structure of RR8 in Coot (43).

SAXS

SAXS data were collected at the SAXS/WAXS beamline at the Australian Synchrotron. Using the co-flow setup, 80 μL of RR8 at 2.7 mg/mL was eluted from a Superdex 200 Increase 5/150 GL column, equilibrated with 50 mM Tris (pH 8.0), 150 mM NaCl, 1.5% v/v glycerol, and in-line with the x-ray beam. Data quality and the initial assessment were conducted using the

Scatterbrain software developed at the Australian Synchrotron (Stephen Mudie, Australian Synchrotron). Further data analysis was conducted using the ATSAS 3.0.4 software package (49). Chromixs was used to assess the SEC-SAXS data and select frames corresponding to buffer and sample (50). Subtracted data were analyzed using Primus to calculate the Rg and Gnom to calculate $P(r)$ (49), ab initio shape determination was performed using Dammif, followed by Damaver and Damfilt (51), Crysol was subsequently used to fit the models of RR8 to the scattering data, calculating both χ^2 and *CorMap* values (49,52). The RR8 model with the CTR was then superimposed onto the SAXS bead model using Supalm within the SASpy plug-in for PyMol (53).

Sequence conservation analysis

One hundred and eighty-three Reelin orthologs were identified using the Ensembl genome browser (54) and analyzed using Jalview (55) to extract amino acid consensus percentages in the loops of interest. WebLogo (56) was used to create the sequence logos for all Reelin repeats displayed in Fig. S3.

Electrostatic surface potential analysis

The electrostatic surface potentials of RR6 (PDB: 2E26, residues 2320–2663) and RR8 (PDB: 7LYU, chain B) were calculated using the APBS Electrostatics (57) plug-in available in PyMol version 2.5.2 (Shrödinger, New York, NY, USA).

ELISA-based binding assay

Ninety-six-well plates were coated with 250 ng of purified proteins in each well. Wells were washed three times with PBS-T, and then blocked with 5% milk in PBS. Plates were then incubated with corresponding concentrations of purified Fc-receptor and 2 μL monoclonal mouse antihuman IgG1-HRP (2 mg/mL; Serotec; Raleigh, NC) for 3.5 h at room temperature. Plates were washed three times with 20 mM Hepes (pH 7.4), 150 mM NaCl, 2 mM $CaCl_2$, and 2 mM $MgCl_2$, and 100 μL 1-Step Ultra TMB-ELISA HRP substrate was then added to each well. Detection of binding was assessed through visualization of the color shift, and the ABS 650 nm was measured. The experiment was conducted in technical triplicate. Statistical analysis was performed using Graphpad Prism8 software (San Diego, CA, USA). The data did not pass the Shapiro-Wilk test for normality (=0.05) and therefore were analyzed nonparametrically using the Kruskal-Wallis test and Dunn's multiple comparisons test. Differences were considered statistically significant when $p \leq 0.05$.

RESULTS

Purification of RR8

RR8 purifies as a single, symmetric peak in SEC, eluting at a volume consistent with a molecular weight (MW) of ~50 kDa when compared with a globular gel filtration standard, suggesting that the protein exists as a monomer in solution (Fig. 2 *A*). Virtually no aggregation is present in the freshly purified and concentrated protein. Assessing the integrity of the protein preparation by SDS-PAGE followed by Coomassie staining shows the protein migrates, as expected, as a single band of ~50 kDa (Fig. 2 *B*).

Crystal structure of RR8

Purified RR8 at ~10 mg/mL crystallized in space group P 1 2_1 1 at a resolution of 3.0 Å (Fig. 2 *C*). The final R_{work} and R_{free} values were 22.7 and 26.4%, respectively (Table 1). Two macromolecular chains (A and B) are present in the asymmetric unit and display noncrystallographic symmetry about a rotational axis of 180° that aided in refinement. Chains A and B were modeled between residues E3053 and S3430 with the exceptions of D^{3064}DEGSSH^{3070}, K^{3100}KD^{3102}, and G^{3213}EET^{3216} on chain A and E^{3066}GSSH^{3070} and $K^{3101}D^{3102}$ on chain B (Fig. 2 *C*). Two putative N-linked glycans were modeled on each chain at N3185 and N3412, whereas sugar chains at the remaining two sites (N3073 and N3439) were not modeled, as they were not clearly resolved (Figs. 2 *C*, 3 *A*, and S1).

As seen in the primary and tertiary structures of other RRs, RR8 can be divided into two subrepeats, A and B, which are linked by an EGF-like domain of 33 residues. The observed jelly-roll-like fold of each subrepeat is also largely similar to those observed in the crystal structures of RRs 1, 3, 5, and 6, as it is made of 11 β-strands that form 2 β-sheets, one convex and the other concave. Two calcium binding sites were apparent in the electron density, and the ions were placed in the model, each being caged by a trio of electrostatically favorable interactions (Figs. 2 *C*, *right panels* and S1).

Due to unclear electron density, S3430 was the last residue that could be confidently placed into the model, leaving 25 amino acids of the CTR unaccounted for (31 if including the 6-residue peptide that is cleaved after the Furin site) (Fig. 2 *C*). To indirectly address this missing piece in the electron density, we expressed an RR8 mutant with an altered Furin recognition site (RRRR to RRAA) to abolish the endogenous cleavage that occurs. SDS-PAGE, followed by western blotting of RR8 WT and RR8 RRAA, show that RR8 WT runs at the expected MW of 50 kDa, while RR8 RRAA runs ~25 kDa larger (Fig. S2 *A*). This is expected since RR8 RRAA is no longer cleaved during expression and retains the C-terminal Fc tag. Given that RR8 RRAA must have an intact CTR and that RR8 WT and RR8 RRAA differ by only 2 amino acids, we infer that the 25 missing residues are included in our crystallized product but are flexible, not packing into an ordered structure that can be modeled due to the highly basic nature of the CTR (see SAXS identification of the CTR).

AUC confirms that RR8 is a monomer in solution

RR8 crystallized with two chains in the asymmetric unit that form an interface of 783.1 Å^2 in area, corresponding to just 2.4% of the two protein chains' total surface area (Fig. 3 *A*). Although the SEC elution profile suggests that RR8 is monomeric in solution (7.4 mg/mL was loaded onto the column, Fig. 2 *A*), to rule out the possibility of physiologically important dimerization we analyzed the structure using the web server, PDBePISA, which identified no likely, biologically relevant interfaces. To further confirm that the observed interface is a product of crystal

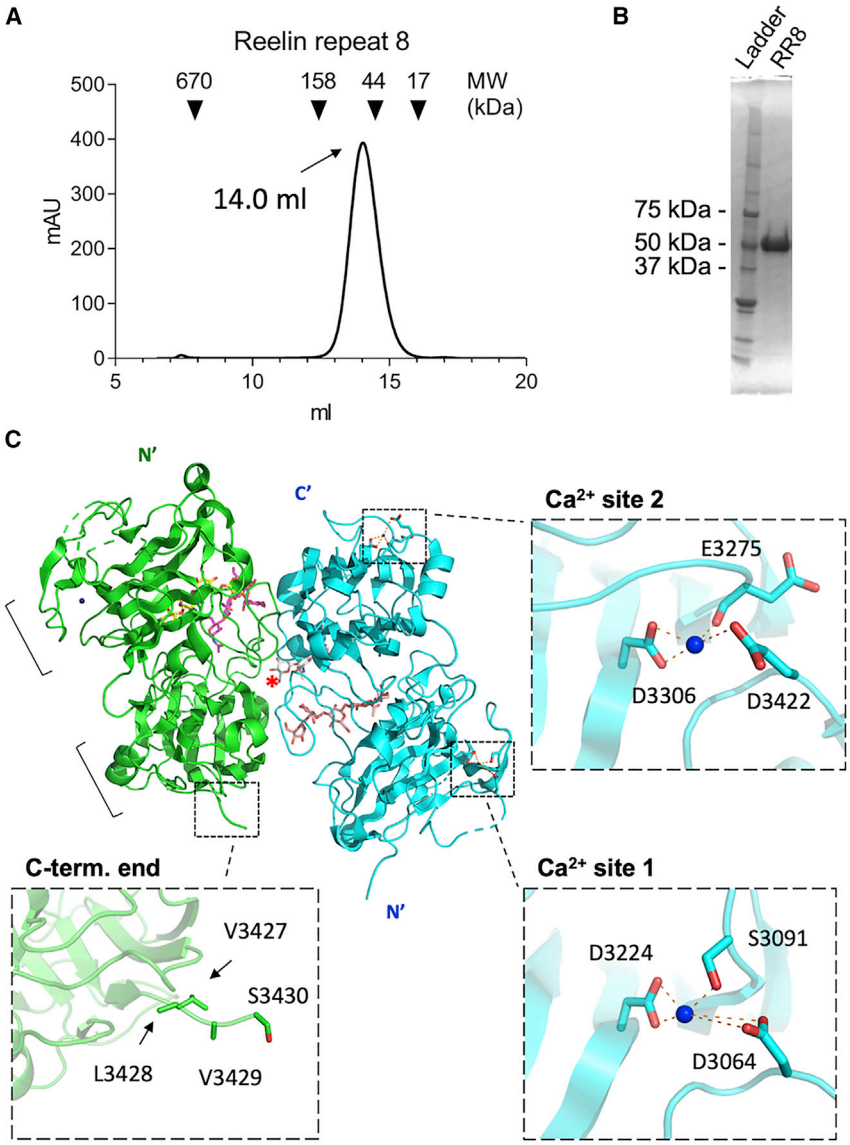

FIGURE 2 Purification and crystal structure of RR8. (*A*) RR8 elutes as a single, symmetric peak corresponding to ∼50 kDa when compared with globular gel filtration standards on a Superdex 200 10/300 GL column. (*B*) SDS-PAGE followed by Coomassie staining in reducing conditions further shows that RR8 runs as a single band at 50 kDa. (*C*) The asymmetric unit of the solved crystal structure is composed of two chains, A (*green*) and B (*cyan*), and each chain comprises two subrepeats (*brackets*). The two chains exhibit noncrystallographic symmetry of 180° about a rotational axis (*asterisk*). Four N-linked glycans are represented as sticks, located on the back of model from the current perspective. Bottom left: the C-terminus of the crystal structure ends at residue S3430. Residues L3428 and V3429 were truncated at Cβ due to ill-defined electron density. Right: two Ca^{2+} ions are modeled on each chain (shown for chain B) as allowed by obvious electron density and coordination by electrostatically favorable interactions.

packing and not present in solution, we performed sedimentation velocity experiments. Experiments conducted at three different protein concentrations, corresponding to 0.1, 0.3, and 0.9 OD, show that RR8 consistently sediments as a single component at a value of 3.6 S, highlighting both the purity of the sample and the lack of concentration-dependent oligomerization (Fig. 3 *B*). Macromolecules of 49.6 and 52.6 kDa account for 99.3% of the measured signal (Fig. 3 *C*), unequivocally showing that RR8 exists solely as a monomer in solution, having a theoretical MW of 46.7 kDa (51.6 kDa with the four putative N-linked glycans accounted for). The AUC-determined frictional ratio (*f*/*f*0) is 1.43, reflecting the asymmetry of the monomer in the crystal structure (Fig. 3 *C*). Modeling the in-solution assembly of the RR8 crystal structure shows that it is elongated with the overall dimensions of 60 × 35 × 30 Å (Fig. 3 *D*).

SAXS identification of the CTR

To further confirm the crystallography and AUC results, SEC-SAXS was performed on purified RR8; the linear Guinier region is indicative of a monodisperse sample with no detectable aggregation (Fig. S2 *B*). The concentration loaded onto the SEC column immediately before data collection was 2.4 mg/mL. The radius of gyration (R_g = 25.0 Å), maximum dimension (D_{max} = 84.9 Å), and MW range (MW = 36.5–40.7 kDa) support the previously observed data, characterizing RR8 as a monomeric protein in solution (Table S1 and Fig. S2 *C*). The dimensionless Kratky plot is bell shaped, confirming that the protein is folded (Fig. S2 *D*). A critical eye will notice that the $P(r)$ is bell shaped, typical of a globular protein, but with a right-handed shoulder that brings the D_{max} to ∼85 Å, which is ∼25 Å larger than the longest dimension measured in the

TABLE 1 Crystallographic data collection and refinement statistics

	Reelin repeat domain 8
Data collection	
Space group	P 1 2_1 1
Cell dimensions	
a, *b*, *c* (Å)	60.171, 104.059, 67.615
α, β, γ (°)	90, 104.109, 90
Resolution (Å)	45.12–3.00 (3.18–3.00)
R_{sym} (%)	15.5 (81.7)
$<I>/<\sigma I>$	5.5 (1.3)
$CC_{½}$	98.5 (49.6)
Completeness (%)	99.9 (99.9)
Redundancy	3.6 (3.5)
Refinement	
Resolution (Å)	45.12–3.00 (3.11–3.00)
Reflections	16,240 (1607)
R_{cryst} (%)	22.71
R_{free} (%)[a]	26.35
Number of atoms	
Protein	5457
Ligands/glycans	226
Average B factors (Å^2)	
All	64.81
Protein	64.31
Ligands/glycans	77.00
RMSD from ideality	
Bond lengths (Å)	0.005
Bond angles (°)	0.900
Geometry	
Ramachandran plot (%)	
Outliers	0.0
Allowed	4.72
Favored	95.28
Rotamer outliers (%)	0.0
Cβ outliers (%)	0.0
All-atom clash score	11.28

[a]5% of reflections was not used during refinement as cross-validation.

crystal structure (~60 Å) (Figs. S2 *C* and 4A). This feature indicates the presence of a second, smaller center of scattering. Consistently, ab initio structure determination revealed a structural envelope that is largely globular with a protuberance at one of the termini (Fig. 4 *A*). We surmised that this projection might represent the CTR that is unaccounted for in our crystal structure. Using a predictive protein modeling software, we modeled a potential tertiary structure of the CTR and manually affixed it to the C-terminus of our RR8 crystal structure. Superimposed, the modified crystal model and SAXS bead model align in a near-perfect manner, with the affixed CTR occupying the protuberance's three-dimensional volume (Fig. 4 *A*). Chi^2 (χ^2) and correlation map test (*CorMap*) values were used to assess the fit of both the ab initio bead model and modified crystal model to the raw SAXS data. With respective χ^2 values of 1.16 and 1.12, the models fit the data and suggest that the CTR forms a conspicuous structural domain adjacent to RR8 (Fig. 4, *B* and *C*). The excellent quality of the scattering data motivated us to further analyze the data, calculating the χ^2 for RR8 without the appended CTR model. With an increased χ^2 of 1.36, the model lacking the CTR does not fit the SAXS data; furthermore, *CorMap* values are increased for this model, and there are obvious deviations where the modeled data points are either consecutively higher or lower than the raw data at low *q* values, indicating a poor fit when compared with both the Dammif model and the model with the attached CTR (Fig. 4, *B–D*).

RR6 and RR8 alignment shows general agreement but altered side-chain orientation at the homologous receptor binding loop

Superimposing the crystal structures of RR6 (residues 2320–2663, PDB: 2E26) and RR8 yields an alignment with an RMSD of 1.6 Å, consistent with the 31.7% sequence identity between the two domains (Fig. 5 *A*). Critical to the Reelin-receptor interaction is residue K2467, which is located on RR6. Through primary structure alignment, it is apparent that a lysine occupies this residue's homologous location on two of the seven other Reelin repeats, RR3 and RR8 (K3218) (Fig. S3). The loop containing this homologous residue is not modeled on the available crystal structure of RR3 (PDB: 2DDU), but the homologous residues are modeled and available for comparison on RR6 and RR8. As expected, K2467 on RR6 adopts a solvent-accessible conformation with its side chain pointing out on the surface of the protein, available for receptor binding. However, K3218 on RR8 has a buried conformation, hidden from any potential intermolecular interactions (Fig. 5 *A*). The residues adjacent to RR6's K2467 compose a distinct patch of hydrophobic residues that is highly conserved in Reelin orthologs (Figs. 5 *B* and S3). In contrast, the residues neighboring K3218 are largely polar, variable among Reelin orthologs, and do not have buried, solvent-inaccessible conformations, thus leaving a pocket available for K3218's side chain to dwell (Figs. 5, *B*, *C* and S3). Distinctively, F2465 in the hydrophobic patch preceding K2467, packs into the homologous pocket that K3218 occupies on RR8 (Fig. 5 *C*). With F2465 snugly fit into this pocket, K2467 (RR6) is now radially oriented and accessible to solvent and protein binding partners (Fig. 5 *D*). The contrasting side chain placement affects the electrostatic potential of the exposed protein surface. K2467 lends a net positive charge to the receptor binding loop, while the homologous surface on RR8 has a net negative charge, as K3218's side chain is not exposed, and a number of acidic residues have side chains that are radially oriented and solvent accessible (Fig. S4). The overall effects of this conformation and the surface electrostatic potential contribute to RR6's physiological importance as K2467 clearly interacts with the calcium coordinating acidic residues on ApoER2 (Fig. 5 *E*). Superimposing RR8 in the context of the ligand-receptor complex (PDB: 5B4X) unambiguously shows K3218's 14.1 Å

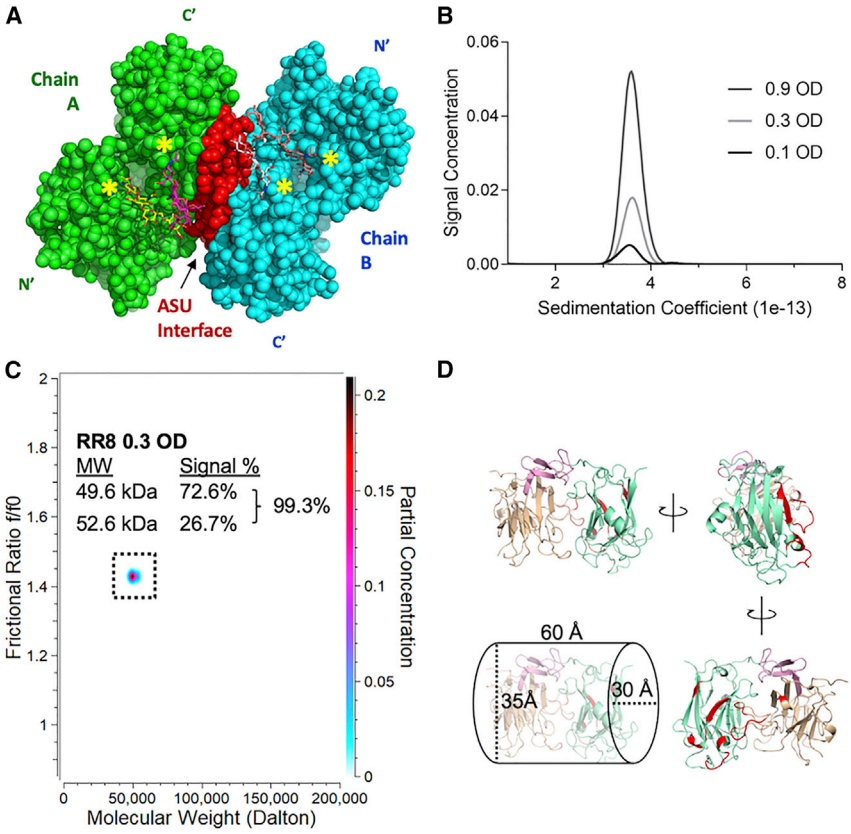

FIGURE 3 RR8 is a monomer in solution. (*A*) Sphere model of RR8 in the asymmetric unit, highlighting the crystallographic interface (*red*) between chains A (*green*) and B (*blue*). Yellow asterisks note the two N-linked glycosylation sites on each chain (N3185 and N3412). (*B*) Sedimentation velocity experiments conducted at 0.1, 0.3, and 0.9 OD (corresponding to 0.063, 0.19, and 0.56 mg/mL, respectively) show that RR8 sediments as a single species of 3.6 S with no evidence of oligomerization. (*C*) Of the signal measured during the sedimentation velocity analysis of RR8 at 0.3 OD, 99.3% is derived from molecular species of 49.6 and 52.6 kDa, both with an *f*/*f*0 of 1.43. (*D*) The crystal structure of RR8 modeled in its monomeric in-solution assembly. The monomer is elongated with its dimensions roughly being 60 × 35 × 30 Å, adopting a cylindrical shape. Subrepeat A is represented in beige; EGF-like domain is in pink; subrepeat B is in aquamarine; artifactually interfacing residues are in red.

displacement and inability to interact with the trio of acidic residues on ApoER2 with which K2467 forms multiple salt bridges (Fig. 5 *E*, dashed line).

Swapping RR6's receptor binding loop into RR8 does not bestow binding capacity

Owing to the high degree of structural alignment between RR6 and RR8 and near identical rotamer states of amino acid residues bordering the loops of interest (Fig. 5 *E*), we aimed to design an RR8 mutant construct with the capacity to bind to the Reelin receptors. We hypothesized that, by swapping the RR6 receptor binding site into the homologous site on RR8, we could introduce a solvent-accessible Lys residue on RR8, bestowing the capacity to bind to the Reelin receptors, ApoER2 and VLDLR (Fig. 6 *A*). Two RR8 mutant constructs (RR8 QQ and RR8 HT) were designed to test the above hypothesis. Both RR8 QQ and RR8 HT express well and after purification migrate at an MW consistent with that of RR8. Like RR8 WT, both constructs elute as a single peak in SEC at ∼14 mL (Fig. 6, *B* and *C*), indicating that overall folding was maintained. However, using an ELISA-based binding assay, we could not detect any significant interaction between either of the mutant RR8 constructs and Reelin receptors, while Reelin's CF provided a robust, positive control (Fig. 6, *D* and *E*). Biolayer interferometry was also negative (data not shown), providing no evidence of binding between the RR8 loop swap constructs and lipoprotein receptors, VLDLR and ApoER2.

DISCUSSION

The three-dimensional structures of several Reelin domains have been published over the years, but despite the increasing focus on RR8 and its adjacent regions, its structure remained unresolved (22,25,28–31,37). Here, we report a crystal structure of RR8 at 3.0 Å resolution, which shows similarities to the other RR structures solved to date but highlights important differences and shows the location and approximate conformation of the CTR.

Using a combination of SEC, SAXS, and AUC, we unequivocally show that RR8 exists as a monomer in solution and that no oligomerization occurs over a ninefold increase in concentration, enabling us to label the observed interface in the crystal structure as artifactual. While it is possible that the high protein concentrations within the crystal drops may create an environment in which dimerization might occur, all in-solution evidence up to 7.4 mg/mL suggests that the protein does not oligomerize. Previous work has shown that, despite Reelin forming a covalently linked homodimer through a disulfide bond on RR5, its flanking domains display some degree of flexibility (23). These data suggest that this flexibility likely extends through to Reelin's

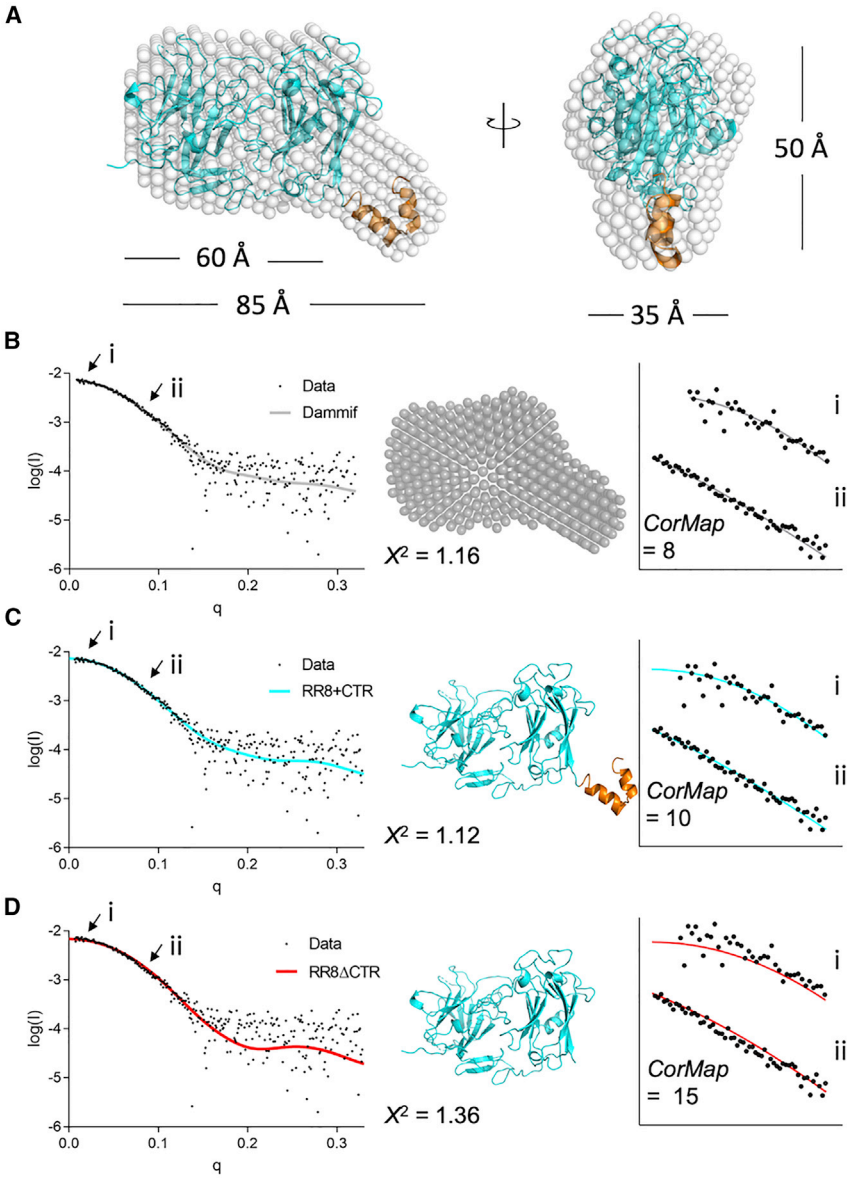

FIGURE 4 Reelin's CTR forms a conspicuous domain adjacent to RR8. (*A*) Superimposition of SAXS Damfilt bead model (*spheres*) and crystal structure of RR8 (*cyan*) with modeled CTR (*orange*). Note the excellent fit of the overlay. (*B*) Ab initio bead model fits the experimental data with a $\chi^2 = 1.16$ ($n = 368$). (*C*) Crysol-calculated fit for the RR8 model with the appended CTR (+CTR) has a $\chi^2 = 1.12$ ($n = 567$). (*D*) Crysol-calculated fit for the RR8 model without the CTR (ΔCTR) has a $\chi^2 = 1.36$ ($n = 567$). Assigning a significance value of $\alpha = 1\%$, the Dammif bead model and RR8+CTR model fit the data with statistical significance, while the RR8ΔCTR model does not. Note the regions of data points that are consecutively positive (*i*) or negative (*ii*) to the fit in farthest right section of (*D*), compared with (*B*) and (*C*). The correlation map test (*CorMap*) values are also shown, representing the largest number of consecutive data points that are either positive or negative to the fit.

C-terminus, as RR8 has no propensity to form a higher-order structure.

RR8 has been of increasing interest to those in the Reelin field, as new developments in its function and regulation have been reported, especially regarding the CTR (26,28,37). Despite not being able to represent the CTR in our crystallographic model of RR8, we confidently identify the region that the CTR occupies using SAXS. The CTR extends off the C-terminus of RR8, forming its own structurally distinct, solvent-accessible domain. While the CTR is likely flexible due to its disproportionately basic composition, structural predictions suggest that the CTR is not completely disordered but does have secondary/tertiary structure. This fits with the current understanding of the CTR, as it has increasingly been shown to serve as a multifunctional domain that not only affects Reelin's secretion and signaling levels but also interacts with the recently reported Reelin binding partner, NRP-1 (26,28,37).

Our recently published structural characterization of Reelin CF shows that it has a maximum dimension of ~245 Å, which is consistent with work from other groups showing that individual repeats are ~60 Å in length (22,23,25,29–31). Our model of RR8 follows this pattern as well as it has a D_{max} of ~60 Å, measured from N-terminus to C-terminus (excluding the CTR). The structure of RR8 shows high agreement when superimposed on the crystal structures of other RRs (RMSD $\leq$ 2.6 Å). Despite the structural similarity, a difference between the receptor binding loop on RR6 (Q^{2461}-Q^{2469}) and its homologous loop on RR8 (Q^{3211}-Q^{3219}) was noteworthy. K2467 on RR6 is critical for the Reelin-receptor interaction and substituting it with an alanine leads to an inert Reelin

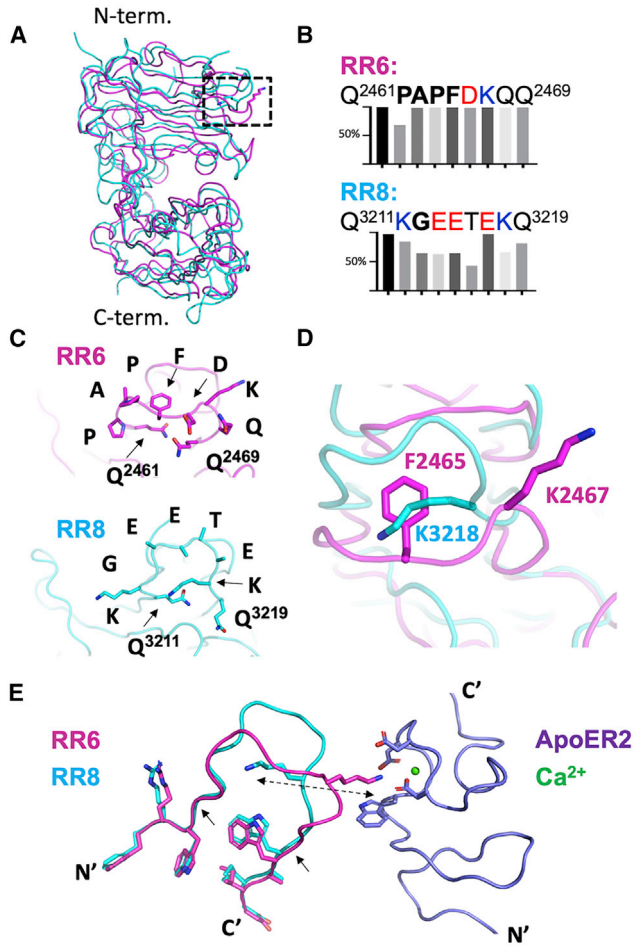

FIGURE 5 Comparison of RR6 and RR8 reveals global similarities but distinct differences. (*A*) RR6 (*magenta*) and RR8 (*cyan*) align with an RMSD of 1.63 Å. Box: outline of homologous residues K2467 and K3218, which are differently positioned and further reported in (*C*) and (*D*). K2467's side chain is radially oriented and solvent exposed, while K3218's side chain is buried into a nearby pocket. (*B*) Sequence comparison and conservation of the homologous loops reveals a highly conserved hydrophobic patch on RR6 that is not present on RR8. Nonpolar residues are bolded; basic residues are represented in blue; acidic residues are in red; polar, uncharged residues are in normal font. (*C*) Comparison of the loops interest. Several residues of RR8 are truncated at Cβ. (*D*) Superimposition of RR6 and RR8 shows that F2465 of RR6 occupies the pocket in which RR8's K3218 is situated. (*E*) The two loops of interest are superimposed and shown in relation to ApoER2. RR6 clearly contacts the calcium coordination site on ApoER2 via K2467. The homologous lysine (K3218) on RR8 is pointed inward, away from any potential interaction with ApoER2. The dashed line highlights K3218's 14.1 Å displacement when compared with K2467, and the arrows signify the approximate boundaries used in the design of the chimeric protein constructs (Fig. 6). The side chains for amino acid residues immediately outside of the boundaries are made visible; they align in near identical rotamers, suggesting the compatibility for a functional replacement of one loop for the other.

construct, unable to initiate canonical pathway activation (23,29,58). Therefore, it is expected that K2467 adopts a solvent-accessible conformation, as seen in the existing crystal structure (PDB: 2E26), available to interact with VLDLR and ApoER2. A homologous lysine residue (K3218) exists in this same position on RR8; however, K3218's R-group is positioned ventrally, buried in a pocket that is occupied by F2465 on RR6. F2465 is part of a highly conserved hydrophobic patch that immediately precedes K2467 on RR6. Other RRs do not share this level of sequence conservation among Reelin orthologs, which argues in favor of evolutionary pressure selecting for this primary structure to maintain the protein's biologically critical interaction with ApoER2 and VLDLR. Unsurprisingly, this affects the superficial electrostatic potential; the surface in the vicinity of the receptor binding loop on RR6 is positively charged (consistent with the salt bridges that occur between Reelin and its receptors), while the homologous region on RR8 has a negative potential.

Given these premises, we hypothesized that swapping RR6's receptor binding loop for RR8's homologous loop may confer an RR8 chimeric protein with the capacity to bind to Reelin receptors. However, despite similar expression and folding, two independent binding assays provided no evidence of interaction between the RR8 loop swap constructs and either ApoER2 or VLDLR. Several possibilities to explain the negative result exist; they include but are not limited to: 1) the changes made in amino acid sequence do not sufficiently mimic the receptor binding site of RR6 to result in detectable binding, 2) unaccounted steric hindrance or repulsive atomic interactions exist and disrupt the interaction between Reelin receptors and the RR8 chimera, or 3) as detailed below, a broader set of secondary and tertiary interactions between Reelin and its receptors are necessary for a stable interaction. We speculate that, given the hydrophobic patch in the immediate vicinity of K2467 and the near identical rotamer states of amino acid side chains bordering the loops of interest (Fig. 5), the chimeric proteins likely present the receptor binding lysine residue in a solvent-accessible conformation and mimic RR6; however, detailed structural information on the loop swap constructs would be necessary to confirm or negate this. Furthermore, in the absence of a chimeric structure, an alignment of RR6 and RR8 and comparison of electrostatic surface potentials reveal no obvious residues on RR8 that would hinder the interaction between the chimeric protein and ApoER2. It is possible that the surrounding residues within RR8 modulate the structure and dynamics of the loop in question, so, despite the apparent similarities between RR6 and RR8, they may be dynamically different. While B factors often serve as a measure of movement and dynamics in x-ray crystallography data, the differing resolutions in the structures available for RR6 and RR8 limit one's ability to compare B factors between the two models.

Reelin makes at least three contact points with ApoER2 across multiple repeats (30). Two minor contact points are not accounted for in either RR8 QQ or RR8 HT and may be necessary to form a stable Reelin-receptor complex. While the single point mutation K2467A completely disrupts binding between Reelin and its receptors, these

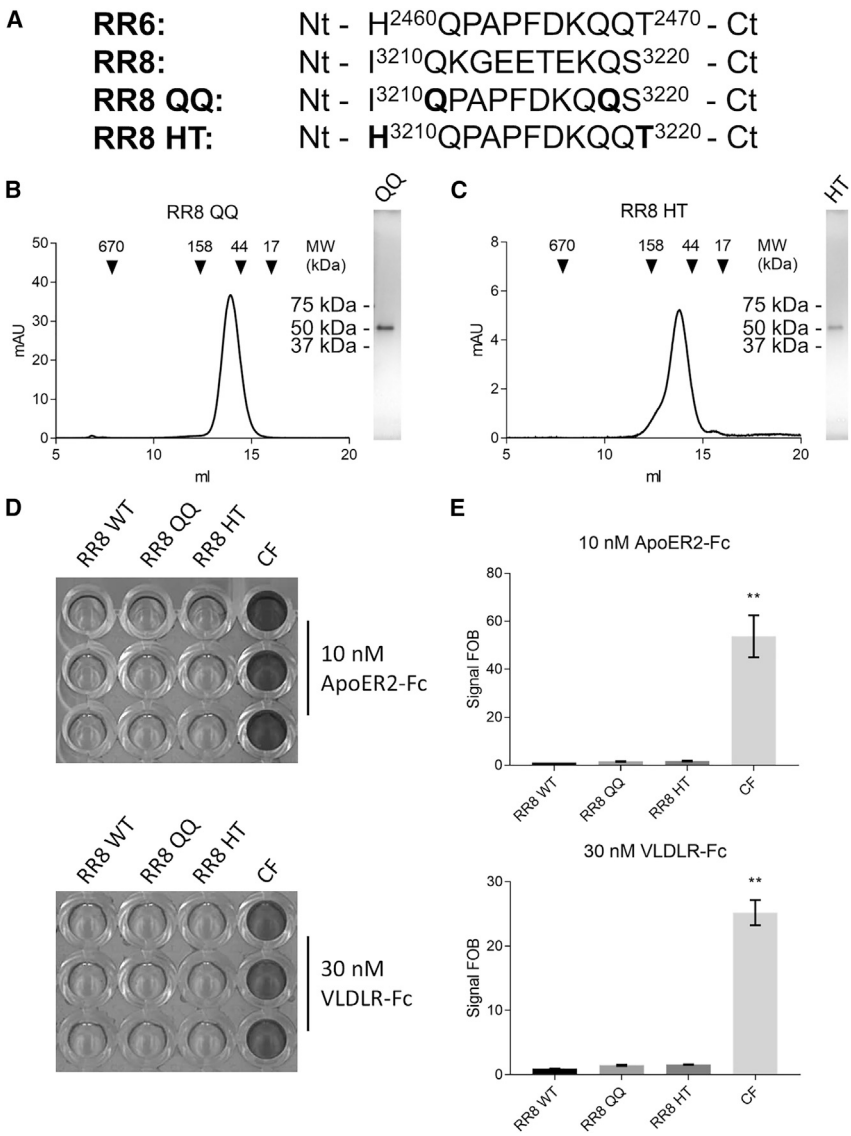

FIGURE 6 RR8 chimeras bind to neither ApoER2 nor VLDLR. (*A*) Amino acid sequence in loop of interest for RR6 and RR8, and the two loop swap constructs, RR8 QQ and RR8 HT. (*B* and *C*) RR8 QQ and RR8 HT elute as single peaks corresponding to ~50 kDa when compared with globular gel filtration standards on a Superdex 200 10/300 GL column. SDS-PAGE followed by Coomassie staining in reducing conditions further shows that both RR8 QQ and RR8 HT run as single bands at 50 kDa. (*D*) ELISA-based binding assay between purified Reelin constructs coating the plate and either ApoER2-Fc at 10 nM (*top*) or VLDLR-Fc at 30 nM (*bottom*). Both experiments were conducted in technical triplicate, and RR8 WT functioned as a negative control, while Reelin's central fragment (CF) served as a positive control. (*E*) Quantification of the ELISAs shows that only the positive control, Reelin CF, elicited a significant increase when compared with RR8 WT for both ApoER2-Fc (*top*) and VLDLR-Fc (*bottom*). In either experiment, no significant difference was observed for RR8 QQ and RR8 HT when compared with RR8 WT. $^{**}p \leq 0.01$.

experiments support a mechanism in which Reelin-receptor binding is a coordinated event across multiple interfaces.

DATA AVAILABILITY

RR8 X-crystallography data reported in this paper are available at PDB: 7LYU.

SUPPORTING MATERIAL

Supporting material can be found online at https://doi.org/10.1016/j.bpj.2022.06.002.

AUTHOR CONTRIBUTIONS

L.S.T. and D.C. conceived the study. All authors designed the experiments. L.S.T. and M.J.C. performed the experiments. L.S.T. and D.C. performed overall data interpretation and co-wrote the manuscript. All authors read and discussed the manuscript.

ACKNOWLEDGMENTS

This work was funded in part by the National Science Foundation, award 1755189, and via strategic research funds from the School of Biological Sciences at Victoria University of Wellington to D.C.; and RWJ Foundation grant 74260 to the Child Health Institute of New Jersey. We thank the support of the NIGMS T32 GM008339 to L.S.T. The content is solely the responsibilities of the authors and does not necessarily represent the official views of the National Institutes of Health. We acknowledge partial funding support for R.C.J.D. and M.J.C. from The Royal Society Marsden Fund (UOC1506). This research was undertaken on the MX1 beamline at the Australian Synchrotron, part of ANSTO.

DECLARATION OF INTERESTS

The authors declare no competing interests.

REFERENCES

1. Borrell, V., J. A. Del Río, …, E. Soriano. 1999. Reelin regulates the development and synaptogenesis of the layer-specific entorhino-hippocampal connections. *J. Neurosci.* 19:1345–1358. https://doi.org/10.1523/jneurosci.19-04-01345.1999.
2. Del Río, J. A., B. Heimrich, …, E. Soriano. 1997. A role for Cajal-Retzius cells and reelin in the development of hippocampal connections. *Nature.* 385:70–74. https://doi.org/10.1038/385070a0.
3. Iafrati, J., M. J. Orejarena, …, P. Chavis. 2014. Reelin, an extracellular matrix protein linked to early onset psychiatric diseases, drives postnatal development of the prefrontal cortex via GluN2B-NMDARs and the mTOR pathway. *Mol. Psychiatr.* 19:417–426. https://doi.org/10.1038/mp.2013.66.
4. Lambert de Rouvroit, C., and A. M. Goffinet. 1998. The reeler mouse as a model of brain development. *Adv. Anat. Embryol. Cell Biol.* 150:1–106.
5. Liu, W. S., C. Pesold, …, E. Costa. 2001. Down-regulation of dendritic spine and glutamic acid decarboxylase 67 expressions in the reelin haploinsufficient heterozygous reeler mouse. *Proc. Natl. Acad. Sci. USA* 98:3477–3482. https://doi.org/10.1073/pnas.051614698.
6. Matsuki, T., R. T. Matthews, …, B. W. Howell. 2010. Reelin and stk25 have opposing roles in neuronal polarization and dendritic Golgi deployment. *Cell.* 143:826–836. https://doi.org/10.1016/j.cell.2010.10.029.
7. Nichols, A. J., and E. C. Olson. 2010. Reelin promotes neuronal orientation and dendritogenesis during preplate splitting. *Cereb. Cortex.* 20:2213–2223. https://doi.org/10.1093/cercor/bhp303.
8. Niu, S., A. Renfro, …, G. D'Arcangelo. 2004. Reelin promotes hippocampal dendrite development through the VLDLR/ApoER2-Dab1 pathway. *Neuron.* 41:71–84. https://doi.org/10.1016/s0896-6273(03)00819-5.
9. Niu, S., O. Yabut, and G. D'Arcangelo. 2008. The Reelin signaling pathway promotes dendritic spine development in hippocampal neurons. *J. Neurosci.* 28:10339–10348. https://doi.org/10.1523/jneurosci.1917-08.2008.
10. Olson, E. C., S. Kim, and C. A. Walsh. 2006. Impaired neuronal positioning and dendritogenesis in the neocortex after cell-autonomous Dab1 suppression. *J. Neurosci.* 26:1767–1775. https://doi.org/10.1523/jneurosci.3000-05.2006.
11. Qiu, S., K. M. Korwek, …, A. PrAttdAvis. 2006. Cognitive disruption and altered hippocampus synaptic function in Reelin haploinsufficient mice. *Neurobiol. Learn. Mem.* 85:228–242. https://doi.org/10.1016/j.nlm.2005.11.001.
12. Rice, D. S., S. Nusinowitz, …, T. Curran. 2001. The reelin pathway modulates the structure and function of retinal synaptic circuitry. *Neuron.* 31:929–941. https://doi.org/10.1016/s0896-6273(01)00436-6.
13. Weeber, E. J., U. Beffert, …, J. Herz. 2002. Reelin and ApoE receptors cooperate to enhance hippocampal synaptic plasticity and learning. *J. Biol. Chem.* 277:39944–39952. https://doi.org/10.1074/jbc.m205147200.
14. D'Arcangelo, G., R. Homayouni, …, T. Curran. 1999. Reelin is a ligand for lipoprotein receptors. *Neuron.* 24:471–479. https://doi.org/10.1016/s0896-6273(00)80860-0.
15. Hiesberger, T., M. Trommsdorff, …, J. Herz. 1999. Direct binding of Reelin to VLDL receptor and ApoE receptor 2 induces tyrosine phosphorylation of disabled-1 and modulates tau phosphorylation. *Neuron.* 24:481–489. https://doi.org/10.1016/s0896-6273(00)80861-2.
16. D'Arcangelo, G., K. Nakajima, …, T. Curran. 1997. Reelin is a secreted glycoprotein recognized by the CR-50 monoclonal antibody. *J. Neurosci.* 17:23–31. https://doi.org/10.1523/jneurosci.17-01-00023.1997.
17. Koie, M., K. Okumura, …, M. Hattori. 2014. Cleavage within Reelin repeat 3 regulates the duration and range of the signaling activity of Reelin protein. *J. Biol. Chem.* 289:12922–12930. https://doi.org/10.1074/jbc.m113.536326.
18. Lambert de Rouvroit, C., V. de Bergeyck, …, A. M. Goffinet. 1999. Reelin, the extracellular matrix protein deficient in reeler mutant mice, is processed by a metalloproteinase. *Exp. Neurol.* 156:214–217. https://doi.org/10.1006/exnr.1998.7007.
19. Ogino, H., A. Hisanaga, …, M. Hattori. 2017. Secreted metalloproteinase ADAMTS-3 inactivates reelin. *J. Neurosci.* 37:3181–3191. https://doi.org/10.1523/jneurosci.3632-16.2017.
20. Sato, Y., D. Kobayashi, …, M. Hattori. 2016. Determination of cleavage site of Reelin between its sixth and seventh repeat and contribution of meprin metalloproteases to the cleavage. *J. Biochem.* 159:305–312. https://doi.org/10.1093/jb/mvv102.
21. Jossin, Y., N. Ignatova, …, A. M. Goffinet. 2004. The central fragment of Reelin, generated by proteolytic processing in vivo, is critical to its function during cortical plate development. *J. Neurosci.* 24:514–521. https://doi.org/10.1523/jneurosci.3408-03.2004.
22. Nogi, T., N. Yasui, …, J. Takagi. 2006. Structure of a signaling-competent reelin fragment revealed by X-ray crystallography and electron tomography. *EMBO J.* 25:3675–3683. https://doi.org/10.1038/sj.emboj.7601240.
23. Turk, L. S., X. Kuang, …, D. Comoletti. 2021. The structure-function relationship of a signaling-competent, dimeric Reelin fragment. *Structure.* 29:1156–1170.e6. https://doi.org/10.1016/j.str.2021.05.012.
24. Yasui, N., Y. Kitago, …, J. Takagi. 2011. Functional importance of covalent homodimer of reelin protein linked via its central region. *J. Biol. Chem.* 286:35247–35256. https://doi.org/10.1074/jbc.m111.242719.
25. Nagae, M., K. Suzuki, …, J. Takagi. 2020. Structural studies of reelin N-terminal region provides insights into a unique structural arrangement and functional multimerization. *J. Biochem.* 169:555–564. https://doi.org/10.1093/jb/mvaa144.
26. Kohno, T., K. Ishii, …, M. Hattori. 2020. Reelin-Nrp1 interaction regulates neocortical dendrite development in a context-specific manner. *J. Neurosci.* 40:8248–8261. https://doi.org/10.1523/jneurosci.1907-20.2020.
27. Ha, S., P. P. Tripathi, …, D. R. Beier. 2017. C-terminal region truncation of RELN disrupts an interaction with VLDLR, causing abnormal development of the cerebral cortex and Hippocampus. *J. Neurosci.* 37:960–971. https://doi.org/10.1523/jneurosci.1826-16.2016.
28. Kohno, T., T. Honda, …, M. Hattori. 2015. Importance of Reelin C-terminal region in the development and maintenance of the postnatal cerebral cortex and its regulation by specific proteolysis. *J. Neurosci.* 35:4776–4787. https://doi.org/10.1523/jneurosci.4119-14.2015.
29. Yasui, N., T. Nogi, and J. Takagi. 2010. Structural basis for specific recognition of reelin by its receptors. *Structure.* 18:320–331. https://doi.org/10.1016/j.str.2010.01.010.
30. Hirai, H., N. Yasui, …, T. Nogi. 2017. Structural basis for ligand capture and release by the endocytic receptor ApoER2. *EMBO Rep.* 18:982–999. https://doi.org/10.15252/embr.201643521.
31. Yasui, N., T. Nogi, …, J. Takagi. 2007. Structure of a receptor-binding fragment of reelin and mutational analysis reveal a recognition mechanism similar to endocytic receptors. *Proc. Natl. Acad. Sci. USA* 104:9988–9993. https://doi.org/10.1073/pnas.0700438104.
32. Copley, R. R., R. B. Russell, and C. P. Ponting. 2001. Sialidase-like Asp-boxes: sequence-similar structures within different protein folds. *Protein Sci.* 10:285–292. https://doi.org/10.1110/ps.31901.
33. Ichihara, H., H. Jingami, and H. Toh. 2001. Three novel repetitive units of reelin. *Brain Res. Mol. Brain Res.* 97:190–193. https://doi.org/10.1016/s0169-328x(01)00307-2.
34. Kubo, K. i., K. Mikoshiba, and K. Nakajima. 2002. Secreted Reelin molecules form homodimers. *Neurosci. Res.* 43:381–388. https://doi.org/10.1016/s0168-0102(02)00068-8.
35. Utsunomiya-Tate, N., K. i. Kubo, …, K. Mikoshiba. 2000. Reelin molecules assemble together to form a large protein complex, which is inhibited by the function-blocking CR-50 antibody. *Proc. Natl. Acad. Sci. USA* 97:9729–9734. https://doi.org/10.1073/pnas.160272497.
36. D'Arcangelo, G., G. G. Miao, …, T. Curran. 1995. A protein related to extracellular matrix proteins deleted in the mouse mutant reeler. *Nature.* 374:719–723. https://doi.org/10.1038/374719a0.

37. Nakano, Y., T. Kohno, …, M. Hattori. 2007. The extremely conserved C-terminal region of Reelin is not necessary for secretion but is required for efficient activation of downstream signaling. *J. Biol. Chem.* 58:S202. https://doi.org/10.1016/j.neures.2007.06.913.

38. Teesalu, T., K. N. Sugahara, …, E. Ruoslahti. 2009. C-end rule peptides mediate neuropilin-1-dependent cell, vascular, and tissue penetration. *Proc. Natl. Acad. Sci. USA* 106:16157–16162. https://doi.org/10.1073/pnas.0908201106.

39. McPhillips, T. M., S. E. McPhillips, …, P. Kuhn. 2002. Blu-Ice and the Distributed Control System: software for data acquisition and instrument control at macromolecular crystallography beamlines. *J. Synchrotron Radiat.* 9:401–406. https://doi.org/10.1107/s0909049502015170.

40. Kabsch, W. 2010. XDS. *Acta Crystallogr. D Biol. Crystallogr.* 66:125–132. https://doi.org/10.1107/s0907444909047337.

41. Evans, P. R., and G. N. Murshudov. 2013. How good are my data and what is the resolution? *Acta Crystallogr. D Biol. Crystallogr.* 69:1204–1214. https://doi.org/10.1107/s0907444913000061.

42. Keegan, R. M., and M. D. Winn. 2008. MrBUMP: an automated pipeline for molecular replacement. *Acta Crystallogr. D Biol. Crystallogr.* 64:119–124. https://doi.org/10.1107/s0907444907037195.

43. Emsley, P., B. Lohkamp, …, K. Cowtan. 2010. Features and development of Coot. *Acta Crystallogr. D Biol. Crystallogr.* 66:486–501. https://doi.org/10.1107/s0907444910007493.

44. Afonine, P. V., R. W. Grosse-Kunstleve, …, P. D. Adams. 2012. Towards automated crystallographic structure refinement with phenix.refine. *Acta Crystallogr. D Biol. Crystallogr.* 68:352–367. https://doi.org/10.1107/s0907444912001308.

45. Laue, T., B. D. Shah, T. M. Ridgeway…, 1992. Computer-Aided Interpretation of Sedimentation Data for Proteins. Analytical Ultracentrifugation in Biochemistry and Polymer Science. Royal Society of Chemistry, Cambridge, UK, pp. 90–125.

46. Brookes, E., W. Cao, and B. Demeler. 2010. A two-dimensional spectrum analysis for sedimentation velocity experiments of mixtures with heterogeneity in molecular weight and shape. *Eur. Biophys. J.* 39:405–414. https://doi.org/10.1007/s00249-009-0413-5.

47. Demeler, B. 2010. Methods for the design and analysis of sedimentation velocity and sedimentation equilibrium experiments with proteins. *Curr. Protein Pept. Sci.* https://doi.org/10.1002/0471140864.ps0713s60.

48. Källberg, M., H. Wang, …, J. Xu. 2012. Template-based protein structure modeling using the RaptorX web server. *Nat. Protoc.* 7:1511–1522. https://doi.org/10.1038/nprot.2012.085.

49. Manalastas-Cantos, K., P. V. Konarev, …, D. Franke. 2021. Atsas 3.0: expanded functionality and new tools for small-angle scattering data analysis. *J. Appl. Crystallogr.* 54:343–355. https://doi.org/10.1107/s1600576720013412.

50. Panjkovich, A., and D. I. Svergun. 2018. CHROMIXS: automatic and interactive analysis of chromatography-coupled small-angle X-ray scattering data. *Bioinformatics.* 34:1944–1946. https://doi.org/10.1093/bioinformatics/btx846.

51. Franke, D., and D. I. Svergun. 2009. DAMMIF, a program for rapid ab-initio shape determination in small-angle scattering. *J. Appl. Crystallogr.* 42:342–346. https://doi.org/10.1107/s0021889809000338.

52. Franke, D., C. M. Jeffries, and D. I. Svergun. 2015. Correlation Map, a goodness-of-fit test for one-dimensional X-ray scattering spectra. *Nat. Methods.* 12:419–422. https://doi.org/10.1038/nmeth.3358.

53. Panjkovich, A., and D. I. Svergun. 2016. SASpy: a PyMOL plugin for manipulation and refinement of hybrid models against small angle X-ray scattering data. *Bioinformatics.* 32:2062–2064. https://doi.org/10.1093/bioinformatics/btw071.

54. Howe, K. L., P. Achuthan, …, P. Flicek. 2021. Ensembl 2021. *Nucleic Acids Res.* 49:D884–D891. https://doi.org/10.1093/nar/gkaa942.

55. Waterhouse, A. M., J. B. Procter, …, G. J. Barton. 2009. Jalview Version 2–a multiple sequence alignment editor and analysis workbench. *Bioinformatics.* 25:1189–1191.

56. Crooks, G. E., G. Hon, …, S. E. Brenner. 2004. WebLogo: a sequence logo generator: figure 1. *Genome Res.* 14:1188–1190. https://doi.org/10.1101/gr.849004.

57. Dolinsky, T. J., J. E. Nielsen, …, N. A. Baker. 2004. PDB2PQR: an automated pipeline for the setup of Poisson-Boltzmann electrostatics calculations. *Nucleic Acids Res.* 32:W665–W667. https://doi.org/10.1093/nar/gkh381.

58. Turk, L. S., D. Mitchell, and D. Comoletti. 2020. Purification of a heterodimeric Reelin construct to investigate binding stoichiometry. *Eur. Biophys. J.* 49:773–779. https://doi.org/10.1007/s00249-020-01465-6.